NUMERICAL AERODYNAMICS AND PERFORMANCE EVALUATION OF A HOVER-CAPABLE AIRSHIP FOR UAM APPLICATIONS USING THE FLIGHTSTREAM SOLVER

Sebastian Oberndorfer, B. Sc., TUM FSD, Munich, Germany
Carlos Hünteler, M. Sc., TUM FSD, Munich, Germany
Hannah Reindle, M. Sc., TUM FSD, Munich, Germany
Florian Holzapfel, Prof. Dr.-Ing., TUM FSD, Munich, Germany
Vivek Ahuja, Altair, Michigan, USA

Abstract

Within the challenging and fast-growing environment of urban air mobility, a hover-capable airship is currently under development to serve as a testbed for Positioning and Guidance Systems. The hover capabilities require a new approach towards 360 ° aerodynamics in the early design stage, to enable accurate model-based controller design. In this paper, the recently developed flow solver FlightStream®, is used to obtain aerodynamic data for a 360° inflow analysis. Using MATLAB as interface, meshing, simulation and post-processing are unified in a framework for easy and quick application. The aerodynamic model is built successfully and integrated in the existing Flight Dynamics Model of the airship. A way to reduce simulation effort by making use of symmetry is presented and employed. The aerodynamic data is found to be accurate in comparison to existing wind-tunnel test data. The solver can robustly handle the airship, and the results presented herein open new possibilities for future usage.

1. NOTATION

Symbols

X	Axial force in body system, N
Y	Side force in body-system, N
Z	Vertical force in body-system, N
L	Rolling moment, Nm
M	Pitching moment, Nm
N	Yawing Moment, Nm
U_∞	Free-stream velocity, $\frac{m}{s}$
V_{ref}	Reference volume, m^3
l_{ref}	Reference length, m

Acronyms:

TUM	Technical University of Munich
FSD	Institute of Flight System Dynamics of TUM
ERF	European Rotorcraft Forum
UAM	Urban Air Mobility
AMI	Air Mobility Initiative
PGS	Positioning & Guidance Systems
FMM	Fast Multipole Method

2. INTRODUCTION

In the fast growing environment of Urban Air Mobility (UAM), new approaches are constantly introduced to overcome limitations and further push innovation. One of the latest projects at TUM-FSD, the AMI initiative, is building an airship, the AMI-PGS. This hover-capable airship is intended to serve as a testbed for Positioning and Guidance sensor Systems (PGS). Their performance in an urban environment shall be analyzed. Compared to other vehicles in the UAM environment, a certification for the airship for flight over populated areas can be achieved with ease. For the airship development, analyses must be carried out ahead and a suitable flight controller is to be built. Both these tasks rely on a precise modeling of the airship. Due to the hover-capabilities in combination with high sensitivity against wind, “classical” aerodynamic approaches are not valid anymore, marking the need for a new approach that can represent all possible flow directions. The implementation of such an approach is the focus of this work, which will present such a model readily for use. A short review on the possibilities currently available and why they are not applicable is given. Then, the software used herein, FlightStream® is introduced and its main features and working principle are described. The environment in which the simulation is carried out is shown briefly. Results are presented for two configurations of the airship, namely a cross-configuration with four fins and a lambda-configuration with three fins. Validation of results is carried out using wind-tunnel data.

3. THE NEED FOR A NEW APPROACH

Aerodynamic modeling of airships still mainly relies on results dating back to the 1920s. Maxwell M. Munk in Ref. 1 first introduced analytic formulations for the forces and moments on an airship's hull, however under the assumption of inviscid flow. Allen and Perkins extended his formulations to include viscous effects, described in various publications (Refs. 2, 3). In 1983, Jones and DeLaurier published their work on aerodynamic estimation for airships (Ref. 4), which still serves as benchmark in today's airship development. They focused on the influence of the fins and furthermore proposed methods to estimate the rotational damping. Their approach is used in the recent works of Mueller (Ref. 5) and Atyya (Ref. 6). However, this approach is still limited to small flow angles and therefore generally only valid in forward flight, making it unsuitable for the specific requirements of the airship considered in this paper. Other authors recently tried with success to use a panel-method based inviscid flow solver on airship configurations (Refs. 7, 8), however this again brings up the limitation of not considering viscous effects. A wealth of research was also performed at the University of Stuttgart in Germany more recently, where besides the analytic model, also a simulation approach was presented that combines an inviscid flow solver with a boundary layer solver. This method enhances the inviscid solution with viscous effects allowing for a more precise estimation (Ref. 9). This method is most promising besides using full-scale CFD simulations. The latter is usually no option in early design stages due to extensive numerical cost. Recent developments at Research in Flight LLC lead to the commercial software package FlightStream®, that makes use of the approach of coupling an inviscid flow solution with a boundary layer solution. Its general buildup and capabilities are introduced in the following.

4. THE FLIGHSTREAM SOLVER

FlightStream® is a highly efficient compressible-flow, viscous, surface-vorticity panel-method flow solver (Ref. 10). It allows for rapid analysis of unconventional aircraft using a unique surface vorticity, flow-separation & viscous analysis capability for both powered and unpowered configurations. As part of prior NASA and AFWERX SBIR/STTR 2018-23 funded activities (Refs. 11, 12, 13, 14, 15) Research in Flight has developed the FlightStream® flow solver to make use of surface vorticity on an unstructured surface. The solver utilizes the Fast Multipole Method (FMM) (Ref. 11). Originally developed for the generalized $n-body$ problem in gravitational fields (Ref. 11), it has been applied in other potential-driven mathematical problems as well, such as in electro-static and potential-flow methods (Ref. 11). The general implementation of FMM in any problem revolves around the coalescing of far-field potential inviscid source/doublet bodies into a single body for evaluation of the net effect on a near-field body (Ref. 11). The algorithm evaluates the inductive effect of near-field bodies identically to the $O(n^2)$-numerical implementation but converts the large number of far-field bodies into a reduced number of clustered bodies inducing an effect based on the sum of their field strengths. In FlightStream®, FMM implementation coalesces far-field vorticity into localized three-dimensional point doublets encompassing the net vorticity strengths of all the coalesced far-field vorticity panels. For viscous analysis, FlightStream® offers laminar and turbulent boundary layer models. The turbulent boundary layer model developed by Standen (Ref. 11) is used. For the fluid properties outside the boundary layer, the flow is assumed to be isentropic and subsonic, but compressible. The presence of both laminar and turbulent separation models in FlightStream® allow for the possibility to model complex transitional separation physics along a given surface streamline. A suitable transition model is required to determine the location where a switch between the laminar and turbulent separation models can be performed. FlightStream® includes the model created by Dvorak *et.al.* (Ref. 11) as the transition model. A robust model for computing attachment lines and critical points on the inviscid surface velocity fields is used to compute flow separation. Using the inviscid surface velocity field, the method developed by Kenwright

(Refs. 12, 13) is used to locate the attachment lines. To perform viscous-coupled flow solutions, the boundary layer models are integrated with the inviscid solver via displacement of the inviscid boundary equal to the displacement thicknesses of the local boundary layers. Loads are computed by summing up the pressure distributions (forces and moments) and using the vorticity distributions for drag computations (Ref. 11). The viscous loads are accounted for using momentum deficit calculations in the boundary layer tangential to the surface panels underneath them. FlightStream® offers a variety of other features. However, those are not considered within the scope of this paper.

5. SIMULATION ENVIRONMENT

At TUM-FSD, most simulation tasks are carried out in MATLAB Simulink. A detailed flight dynamics model of the airship is implemented. It allows to simulate the complete non-linear dynamics, as well as implementing all physical phenomena ranging from aerodynamics and propulsion models to subsystem dynamics. The underlaying equations of motion for this particular case are solved at an arbitrary point for a rigid body with added masses, derived from Refs. 16–18. For Open-Loop analysis purposes, an in-house trimming an linearization tool (Ref. 19) is employed. Aerodynamics are typically introduced into this model via look-up tables. This is where the data obtained by FlightStream® simulations is to be embedded. Also, pre- and post-processing is carried out using in-house MATLAB toolboxes, building an agile and self-contained aerodynamics analysis toolchain. The geometry definition is generated within a MATLAB toolbox, but in principle any CAD model can be used in FlightStream. The approach taken, however allows for a quicker adaption to new designs, a great advantage in early development stages. Since FlightStream is scriptable, the simulation runs do not have to be manually started but can also be controlled out of MATLAB.

6. SIMULATION SETUP

6.1. General reference settings

All simulations are carried out at a defined reference speed of $U_\infty = 8\,\frac{m}{s}$, which is the design cruise speed of the airship. Unsteady aerodynamics are not considered. ISA-conditions at mean sea level (MSL) are applied. The definition of the reference geometry differs from classical fixed-wing cases. Herein the reference area is defined to be $S_{ref} = V^{\frac{2}{3}} = 16.98\,m^2$, with V being the hulls volume. This is a common choice for airships (Ref. 20). As reference length, the airships overall length is used, $l_{ref} = 15\,m$, another common choice would be $l_{ref} = V^{\frac{1}{3}}$. The non-dimensional coefficients are calculated as for fixed wing applications (Ref. 20). As mentioned, a fully turbulent boundary layer model is used, leaning on more recent wind-tunnel tests of similar airships (Ref. 21) and work conducted in FlightStream® before (Ref. 22).

The forces and moments or their respective coefficients are represented in the body fixed coordinate frame of the airship. The frame is defined at a reference point, which is the volume center, with the x-axis pointing towards the hulls bow, the z-axis points downwards and the y-axis forming an orthonormal base.

6.2. Meshing of the Configuration

Meshing and subsequently the total number of faces have a great impact on the performance of numerical solvers. Wrong meshing can even result in divergence of the solution. Within FlightStream®, the meshing of the configuration can be set independently of the geometry definition via a built-in meshing tool. This allows to define the geometry very precisely without generating a dense mesh.

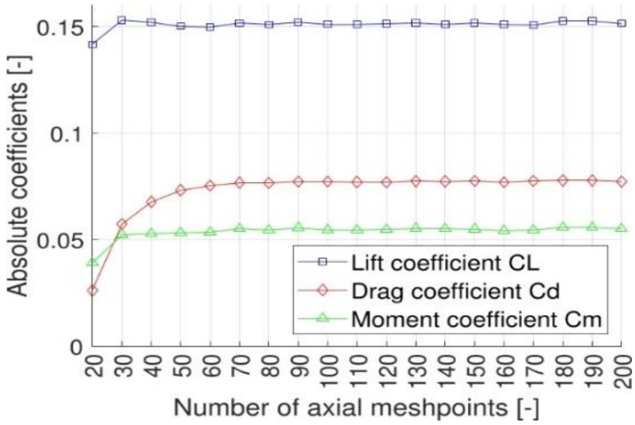

Figure 1: Convergence of coefficients with mesh adaptation

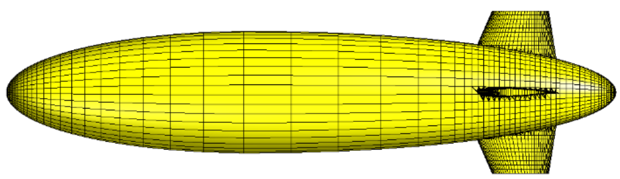

Figure 2: Mesh Configuration of the airship

Variations of the mesh can also be tested this way. Some basic, but by no means exhaustive studies are conducted on the airship to find a reasonable balance between performance and ensuring robust convergence. Similar considerations within the FlightStream® solver have been made by Fei in Ref. 23. For the airship, the simulation is found to be particularly sensitive towards the number of axial mesh faces. A too low number of faces results in a rather pointy and uneven shape within the solver. Viscous effect can no longer be calculated properly, leading to divergence of the entire solution. On the other side, a very high number of faces results in extensive simulation time, which is also not affordable. Figure 1 shows the change in some basic coefficients with the number of faces used. Note that the number of axial mesh points corresponds to the number of mesh faces but is the way meshing is named in FlightStream®. Convergence can be observed from around 80 mesh point towards increasing numbers. Using this result, a mesh is finalized with a total of 13,824 faces, depicted in Figure 2. This corresponds to a simulation time of around 2 minutes per datapoint, which is deemed reasonable for the scope herein, though potential for further reduction is clearly given and may be investigated in further research.

6.3. Symmetry of the Simulation

For most flying configurations, further reduction of simulation time can be achieved by making use of symmetry considerations. The airship considered is at least symmetric around the xz-plane of the body frame, in case of a cross configuration also around the xy-plane. Using this, only half, respectively a quarter of the desired datapoints needs to be simulated. Around the body frame xz-plane, data for forces and moments can be mirrored as follows, creating opposite sideslip angle data:

$$\begin{bmatrix} X \\ Y \\ Z \\ L \\ M \\ N \end{bmatrix}_{-\beta} = \begin{bmatrix} X \\ -Y \\ Z \\ -L \\ M \\ -N \end{bmatrix}_{\beta}$$

The considerations around the xy-plane for the cross-configuration are similar.

6.4. Post-processing of Aerodynamic Data

Naturally to numerical solvers, the raw output data may be peaky due to numerical deviations. This especially poses a problem with very small coefficient values. To reduce the influence of such peaks, a smoothing is applied. A local quadratic regression method is chosen as fitting method. In case of divergence at a single datapoint, though unlikely, the smoothing also “replaces” the missing data by

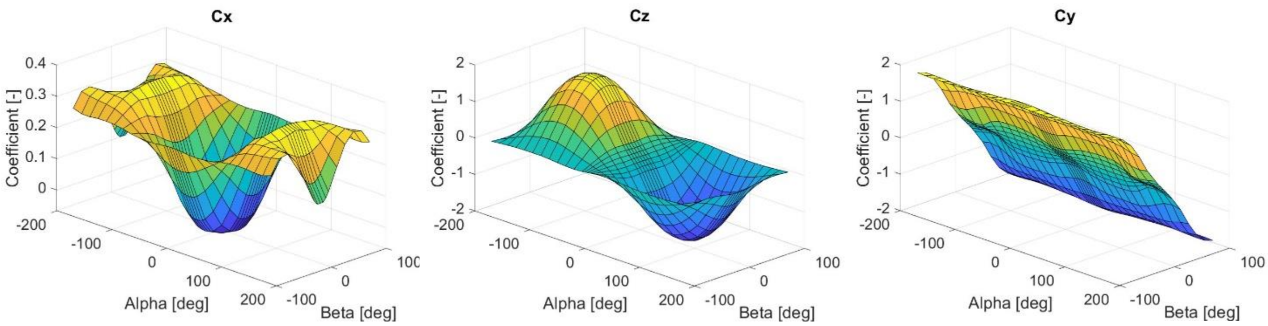

Figure 3 : Body-fixed force coefficients of the airship in cross configuration

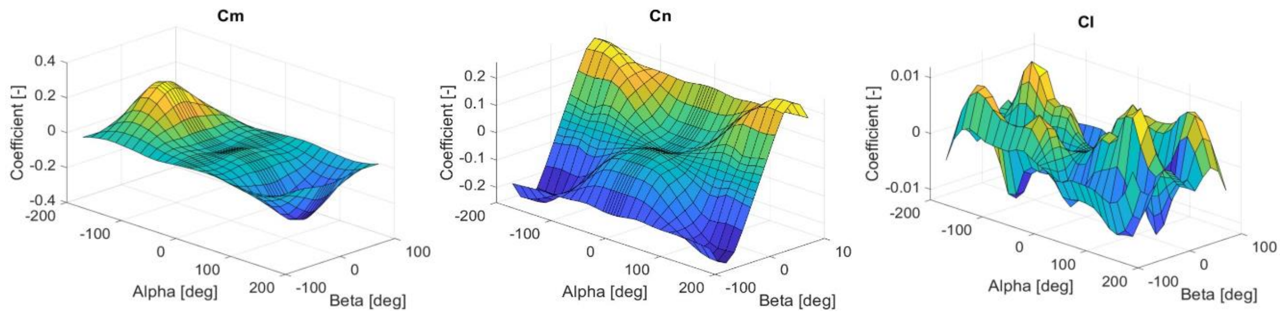

Figure 4 : Body-fixed moment coefficients of the airship in cross-configuration

interpolation of its neighboring points. This makes the results of post-processing more robust against solver divergence, contributing to the overall reliability of the toolchain.

6.5. Performance Simulations

Once the aerodynamic model is integrated in the FDM, the open-loop performance of the whole system can be assessed. The propulsion system of the airship consists of 4 tiltable propellers, placed four meters in front and behind the aircrafts' reference point and two meters to each side of the x-axis. The propeller aerodynamics are calculated with an in-house tool based on Blade Element Momentum Theory as explained in Ref. 24 and not further discussed in this paper. Through the trim routine the behavior inside the whole envelope can be analyzed (Ref. 19). The rotational speed of all propellers as well as their tilting angle are considered to be solver variables. A possible strategy to define a unique solution to the trim problem is to inlcude a cost function. The chosen cost function for the presented analysis is

$$J = \sum_i \omega_i^4.$$

With ω_i the rotational speed of each propeller. The varying trim parameters shown here are the forward an lateral airspeed in the control frame $(u_A^G)_C^E, (v_A^G)_C^E$ and the course change $\dot{\chi}_A^G$.

7. SIMULATION RESULTS

7.1. Cross Configuration

A cross configuration with four fins serves as the first reference case. Figure 3 shows the results for all aerodynamic force coefficients. The solver indeed proved to be very robust, divergence was only detected at a single data point. No dedicated reason for this failure could be found. Due to the smoothing, the single failure point does not affect the overall result. The shapes for the axial force and vertical force indeed look very smooth. Expected behavior like minimal axial force at zero angle of attack and zero angle of sideslip. For the side-force coefficient the shape is remarkable tough. Surprisingly, there is almost no dependency of the crossforce coefficient Cy on the angle of attack. For the moment coefficients, depicted in Figure 4, shapes also match the intuitive expectation for pitching and yawing moment. It can be observed that the rolling moment coefficient is generally very small, as expected for a symmetric configuration. The fact that it is not exactly zero and exhibits some peaks is attributed to numerical residuums of the solver. It should be noted that the values do not compare easily to known dimension for fixed-wing configurations due to the different reference parameters used, as discussed earlier.

To validate the results, a comparison to existing data

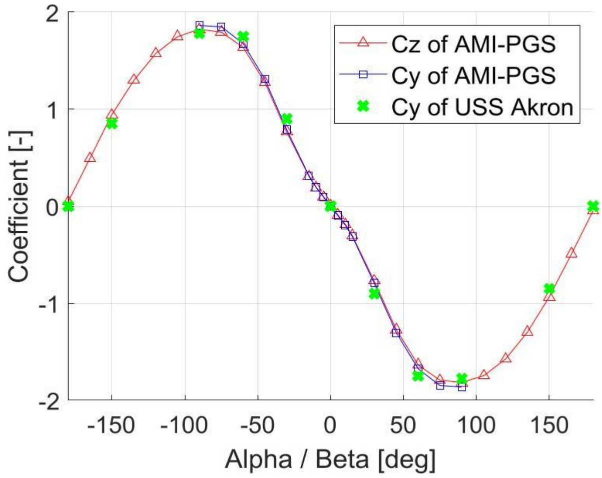

Figure 5 : Comparison of force coefficients of cross-configuration with wind-tunnel data of USS Akron

is appropriate. Using data from the described analytic models in Section 3 however is of course useless as of their inherent drawbacks. Wind-tunnel data is therefore the only reliable source. For comparison, available wind-tunnel data obtained on a 1/40 scale model of the airship USS Akron is used from Ref. 25. For USS Akron, unlike all other sources openly available (Refs. 26–28), data in a range more similar to the one considered herein was recorded. Figure 5 shows

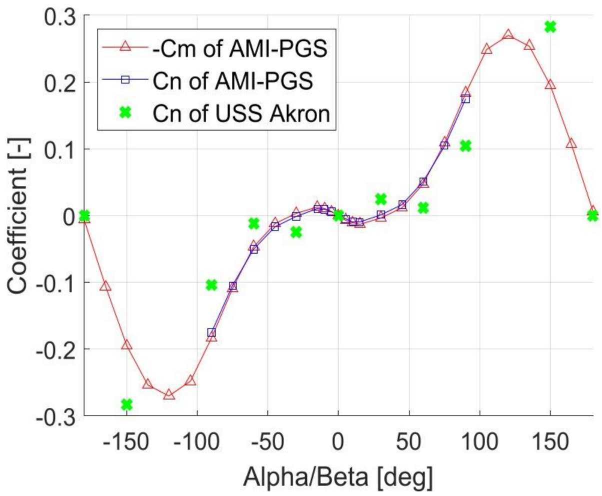

Figure 6 : Comparison of moment coefficients of cross-configuration with wind-tunnel data of USS Akron

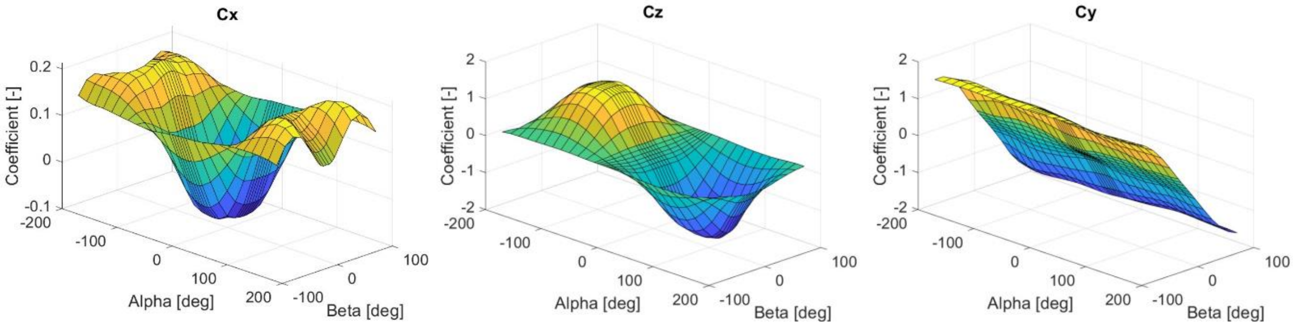

Figure 7 : Body-fixed force coefficients of the airship in lambda-configuration

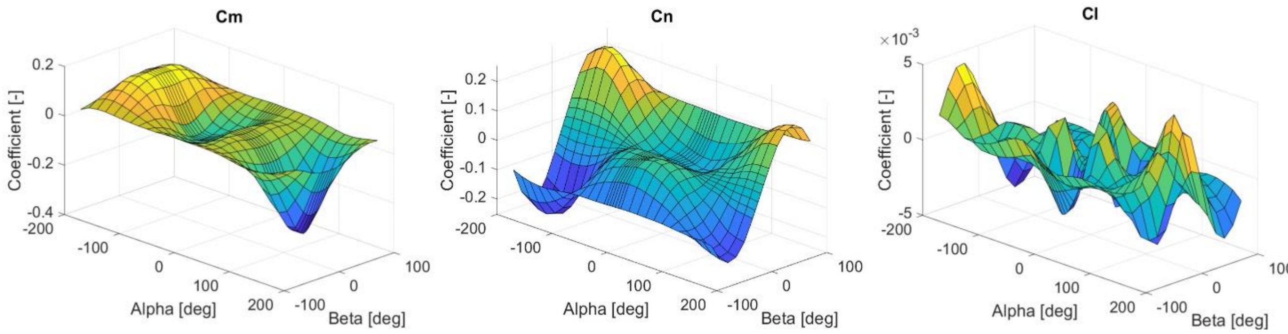

Figure 8 : Body-fixed moment coefficients of the airship in lambda-configuration

the comparison between the vertical force coefficients Cz measured and simulated, respectively. As for all following figures, the flow angle along which a coefficient primarily changes is varied, while the second one is kept zero. The side force coefficient of the simulated data is also included, as it should be equal to the vertical force coefficient due to the symmetry considerations made earlier. The match between all values is excellent over the entire range of flow angles. This also indicates that despite the odd shape for the side-force coefficient discussed above, the force is correctly calculated. For the moments, the comparison is depicted in Figure 6. The pitching moment is inverted to adhere to a different coordinate frame used for USS Akron (Ref. 25). Again, the yawing moment is also depicted for comparison due to its equivalence in symmetric configurations. The match in the data is not as good as for the force coefficients, but still magnitude and qualitative behavior are similar. The only remarkable difference is the fact that the moment coefficients for low absolute flow angles in a range of around -30 to 30 degrees have opposite signs. However, it is a well-known fact that airship exhibit an unstable pitching moment for low angles, stabilizing only with increasing angles (Ref. 29). While this effect is captured in the proper direction in the simulated data, it is not depicted correctly in the wind-tunnel data. This observation is deemed an acceptable deviation, because the absolute numerical deviation is not very large.

7.2. Lambda Configuration

The cross-configuration discussed just above is a suitable testing case for the solver and embedding. A second common design is now considered, a lambda configuration with three fins distributed equally at the hull with one pointing upwards. For this design, no reference data is available tough. This means that the validation must rely solely on the encouraging results of the cross-configuration. For the lambda-configuration, three smaller fins are mounted at the hull, with the first one pointing upwards and the other two being symmetrically distributed on the lower hull. The meshing of the hull is unaffected by this. The solver again performed very robust, this time without a failure at any data point is registered. Figure 7 shows the results for the force coefficients, whilst Figure 8 displays the moment coefficients. The shapes are very similar to the cross-configuration, as most of the aerodynamics is primarily influenced by the hull, which has not been changed. Only the pitching moment coefficient is remarkably smaller. This can be explained due to the reduced number of fins. Also, the axial force coefficient is slightly reduced, indicating lower drag on the fin profile due to smaller fins.

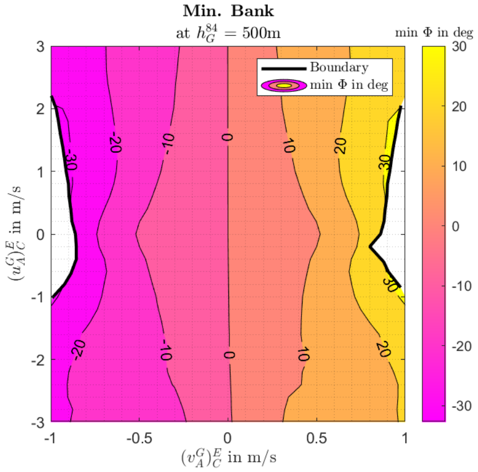

Figure 9 : Minimum Roll angle over horizontal velocity plane for the lambda configuration

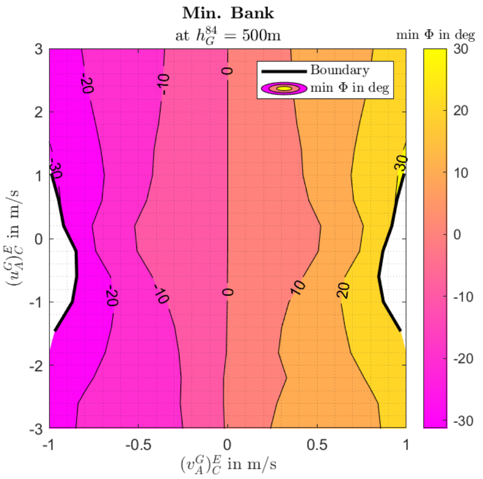

Figure 10 : Minimum Roll angle over horizontal velocity plane for cross-configuration

7.3. Simulation of Control Surfaces

To analyze the effect of the control surfaces, FlightStream® offers a functionality of defining and rotating small surfaces as part of the fins. This makes simulation of control derivatives possible without having to redefine the entire geometry. A slightly refined mesh is applied to the fins due to larger gradients in the geometry resulting from the deflections. Unfortunately, FlightStream® is rather sensitive with respect to deflected surfaces, simulations diverge quickly, especially for increasing flow angles. This is expected to improve with a future version of FlightStream®. However, for zero angle of attack, the delta in the pitching moment coefficient due to control surface deflection is found to match values from wind-tunnel testing of other airships (Ref. 21). Since the control surfaces are only used in forward flight at moderate angles, this value serves as a good initial estimate, as wind-tunnel data also suggests the delta stays constant up to certain flow angles a certain angle range.

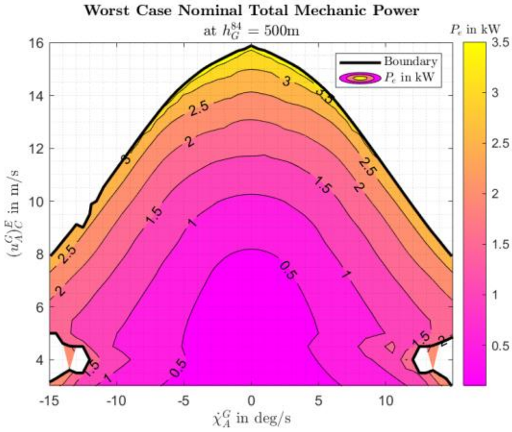

Figure 11 : Total mechanical power consumption over forward speed and course change for the lambda-configuration

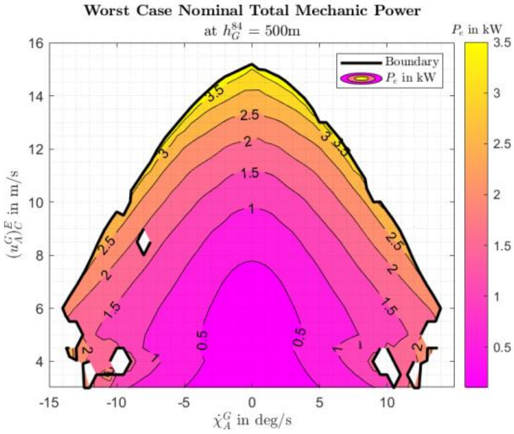

Figure 12 : Total mechanical power consumption over forward speed and course change for the cross-configuration

7.4. Performance Simulations

As explained in Sections 5 and 6.5, the performance of both configurations is compared with an exemplary 2D trim. Figure 9 and Figure 10 show the resulting minimum roll angle for both configurations over the forward and lateral speed. Both configurations present a similar and symmetric behavior for low speed. This highlights the advantage of the 360° aerodynamic model. However, in the high-speed phase, differences in the performance between both configurations can be identified. Figure 11 and Figure 12 depict the total mechanical power over the forward speed and course change envelope. For the lambda configuration, a slightly lower cruise power at $(u_A^G)_C^E = 8\ \frac{m}{s}$ is obtained. Moreover, the maximum achievable speed as well as the maximum turn performance is higher for the lambda configuration. This might be explained by a higher total drag for the cross configuration.

The results prove that with the implemented routine, the influence of the aerodynamic characteristics of a given configuration on the open-loop performance can be analyzed and compared in an automatized manner.

8. CONCLUSIONS

1. A simulation environment is successfully built, including numerous tools to quickly adapt, execute and post-process numerical aerodynamic simulations in the FlightStream® solver. The capabilities of the solver in handling aerodynamics beyond attached flow have been demonstrated

2. Aerodynamic data is successfully simulated for two distinct configurations and comparison with wind-tunnel data shows the validity of the concept presented. Usage of the configuration for performance analysis has been introduced.

3. Future adaptions can be easily integrated into the toolchain, making it a fast and versatile tool in early design stages, by no means restricted to airship cases.

Author contact:

Sebastian Oberndorfer; sebastian.oberndorfer@tum.de

Carlos Hünteler; carlos.huenteler@tum.de

Hannah Reindle; hannah.reindle@tum.de

Florian Holzapfel; florian.holzapfel@tum.de

Vivek Ahuja; vahujua@altair.com

9. Acknowledments

The authors would like to acknowledge that this work emerged within the AMI-PGS project, a part of the AMI initiative, funded by the government of Bavaria. Some of the work was also part of a thesis work of the main author at TUM FSD (Ref. 30).

10. REFERENCES

1. Max M. Munk, *The Aerodynamic Forces on Aiship Hulls*, Washington 184, 1924.
2. J. Allen and E. W. Perkins, *A Study of Effects of Viscosity on Flow over Slender Inlinced Bodies of Revolution: Report 1048*, Ames Aeronautical Laboratory, Moffett Field, Calif., 1951.
3. J. Allen and E. W. Perkins, *Characteristics of flow over inclined bodies of revolution*, Ames Aeronautical Laboratory, Washington, 1951.
4. S. P. Jones and J. D. DeLaurier, *Aerodynamic estimation techniques for aerostats and airships*, Journal of Aircraft, vol. 20, no. 2, pp. 120–126, 1983, doi: 10.2514/3.44840.
5. J. B. Mueller, M. A. Paluszek, and Y. Zhao, *Development of an Aerodynamic Model and Control Law Design for a High Altitude Airship*, 2004.
6. M. Atyya, G. M. ElBayoumi, and M. Lotfy, *Optimal shape design of an airship based on geometrical aerodynamic parameters*, *Beni-Suef Univ J Basic Appl Sci*, vol. 12, no. 1, 2023, doi: 10.1186/s43088-023-00352-1.
7. J. L. Mendonça Junior, J. S. Santos, M. A. Morales, L. C. Goes, S. Stevanovic, and R. A. Santana, *Airship Aerodynamic Coefficients Estimation Based on Computational Method for Preliminary Design*, in *AIAA Aviation 2019 Forum*, Dallas, Texas, 2019.
8. J. Gonzalo, D. Domínguez, A. García-Gutiérrez, and A. Escapa, *On the development of a parametric aerodynamic model of a stratospheric airship*, Aerospace Science and Technology, vol. 107, p. 106316, 2020, doi: 10.1016/j.ast.2020.106316.
9. T. Lutz, P. Funk, A. Jakobi, and S. Wagner, *Summary of Aerodynamic Studies on the Lotte Airship*, Institute of Aerodynamics and Gas Dynamics, University of Stuttgart, Stuttgart, 2002.
10. Research in Flight LLC., *Flightstream User Guide*, 2023.
11. J. E. Burkhalter, V. Ahuja, and R. Hartfield, Robust *prediction of high lift using surface vorticity: NASA SBIR NNX17CL12C, Phase II final report*, 2017.
12. V. Ahuja and R. J. Hartfield, *Aerodynamic Loads over Arbitrary Bodies by Method of Integrated Circulation*, Journal of Aircraft, vol. 53, no. 6, pp. 1719–1730, 2016, doi: 10.2514/1.C033619.
13. V. Ahuja, I. Chakraborty, and R. Hartfield, *Modular Generalized Framework for Assesing Aircraft Aero-Propulsive, Stability and Control Characteristics: NASA Transformational Tools & Technologies Transformative (TTT)*

Aeronautics Concepts Program Award, 80LARC19C0013, 2018-21.
14. V. Ahuja, I. Chakraborty, and R. Hartfield, *Air Vehicle Gust Response Analysis for Early Design: NASA Small Business Innovative Research (SBIR) contract Phase II, 80NSSC21C0025*, 2020-22.
15. V. Ahuja, D. Hunsaker, and R. Hartfield, *A Multi-Fidelty Supersonic Flow Solver for Preliminary Desing & Optimization: USAF AFWERX SBIR contract Phase II, FA864922P0081*, 2023.
16. J. R. Azinheira, A. Moutinho, and E. C. de Paiva, *Erratum on "Influence of Wind Speed on Airship Dynamics*", Journal of Guidance, Control, and Dynamics, vol. 31, no. 2, pp. 443–444, 2008, doi: 10.2514/1.33409.
17. P. G. Thomasson, *Equations of Motion of a Vehicle in a Moving Fluid*, Journal of Aircraft, vol. 37, no. 4, pp. 630–639, 2000, doi: 10.2514/2.2645.
18. P. Peddiraju, T. Liesk, and M. Nahon, *Dynamics Modeling for an Unmanned, Unstable, Fin-Less Airship*, in 18th AIAA Lighter-Than-Air Systems Technology Conference, Seattle, Washington, 2009.
19. M. Weingartner, J. Lenz, G. Sachs, and F. Holzapfel, *Object Oriented Trim of Complex High-Fidelity Simulation Models*, in AIAA Modeling and Simulation Technologies Conference and Exhibit, Hilton Head, South Carolina, 2007.
20. G. E. Carichner and L. M. Nicola, *Fundamentals of aircraft and airship design: Volume 2 - airship design and case studies*. Reston, VA: AIAA (American Institute of Aeronautics and Astronautics), 2013.
21. P. Funk, T. Lutz, and S. Wagner, *Experimental investigations on hull-fin interferences of the LOTTE airship*, *Aerospace Science and Technology*, vol. 7, no. 8, pp. 603–610, 2003, doi: 10.1016/S1270-9638(03)00058-0.
22. G. A. DiMaggio, R. J. Hartfield, and V. Ahuja, *Rapid Prediction of Hybrid Wing Body Aerodynamics*, in *AIAA AVIATION 2022 Forum*, Chicago, IL & Virtual, 2022.
23. Xiaofan Fei, *Evaluation of a Commercial Surface Vorticity Flow Solver for the Modeling of Propeller-Wing Interaction*, NASA Langley Research Center, Hampton, VA, 23681, USA, 2019.
24. N. Bähr, *Modeling of the Rotor Blade Flapping Motion of a Transition Aircraft*, Thesis, FSD, Technische Universität München, München, 2018.
25. A. Silverstein and B. G. Gulick, *Ground-Handling Forces on a 1/40 -Scale Model of The U. S. Airship "Akron"*, Report No. 566, National Advisory Comittee for Aeronautics, 1936.
26. H. B. Freeman, *Force Measurements on a 1/40-Scale Model of The U.S. Airship "Akron"*, Report No. 432, National Advisory Comittee for Aeronautics, 1932.
27. S. B. V. Gomes, *An Investigation of the Flight Dynamics of Airships with Application to the YEZ -2A,* PhD Thesis, College of Aeronautics, Aerodynamics Department, Cranfield Institute of Technology, Cranfield, 1990.
28. I. H. Abbott, *Airship Model Tests In The Variable Density Wind Tunnel*, Report No. 394, National Advisory Comittee for Aeronautics, 1931.
29. B. G. Kämpf, *Flugmechanik und Flugregelung von Luftschiffen*. Zugl.: Stuttgart, Univ., Diss., 2003 (Nicht für den Austausch). München: Utz, 2004.
30. S. Oberndorfer, *Aerodynamic Simulation and Performance Analysis of the AMI-PGS Airship*, Thesis, FSD, Technische Universität München, München, 2024.

Gefördert durch

Bayerisches Staatsministerium für Wirtschaft, Landesentwicklung und Energie